AFRL-AFOSR-JP-TR-2023-0086

Design of refractory high entropy superalloys: from critical phase information to theory development

Ming-Hung Tsai
NATIONAL CHUNG HSING UNIVERSITY
145, HSINGDA RD.,
SOUTH DIST.,
TAICHUNG CITY, , 40227
TWN

06/23/2023
Final Technical Report

DISTRIBUTION A: Distribution approved for public release.

Air Force Research Laboratory
Air Force Office of Scientific Research
Asian Office of Aerospace Research and Development
Unit 45002, APO AP 96338-5002

REPORT DOCUMENTATION PAGE

PLEASE DO NOT RETURN YOUR FORM TO THE ABOVE ORGANIZATION.

1. REPORT DATE	2. REPORT TYPE	3. DATES COVERED	
20230623	Final	START DATE 20200930	END DATE 20220329

4. TITLE AND SUBTITLE
Design of refractory high entropy superalloys: from critical phase information to theory development

5a. CONTRACT NUMBER	5b. GRANT NUMBER	5c. PROGRAM ELEMENT NUMBER
	FA2386-20-1-4086	
5d. PROJECT NUMBER	**5e. TASK NUMBER**	**5f. WORK UNIT NUMBER**

6. AUTHOR(S)
Ming-Hung Tsai

7. PERFORMING ORGANIZATION NAME(S) AND ADDRESS(ES)
NATIONAL CHUNG HSING UNIVERSITY
145, HSINGDA RD.,
SOUTH DIST.,
TAICHUNG CITY 40227
TWN

8. PERFORMING ORGANIZATION REPORT NUMBER

9. SPONSORING/MONITORING AGENCY NAME(S) AND ADDRESS(ES)	10. SPONSOR/MONITOR'S ACRONYM(S)	11. SPONSOR/MONITOR'S REPORT NUMBER(S)
AOARD UNIT 45002 APO AP 96338-5002	AFRL/AFOSR IOA	AFRL-AFOSR-JP-TR-2023-0086

12. DISTRIBUTION/AVAILABILITY STATEMENT
A Distribution Unlimited: PB Public Release

13. SUPPLEMENTARY NOTES

14. ABSTRACT
In this work, 14 alloys in two refractory high entropy alloy systems were investigated. The equilibrium microstructure, phase constituents, and compositions of phases of each alloy after prolonged annealing at three different temperatures were unraveled. The partial pseudo-ternary phase diagram of the two systems at three temperatures was depicted according to the compositions of phases. Based on the phase diagrams, the B2 phase regions were also evaluated.

15. SUBJECT TERMS

16. SECURITY CLASSIFICATION OF:			17. LIMITATION OF ABSTRACT	18. NUMBER OF PAGES
a. REPORT	b. ABSTRACT	c. THIS PAGE		
U	U	U	SAR	32

19a. NAME OF RESPONSIBLE PERSON	19b. PHONE NUMBER *(Include area code)*
JEREMY KNOPP	315-227-7006

Standard Form 298 (Rev.5/2020)
Prescribed by ANSI Std. Z39.18

DISTRIBUTION A: Distribution approved for public release.

- **Federal Agency and Organization Element to Which the Report is Submitted**
  ASIAN OFFICE OF AEROSPACE R&D
- **Federal Grant or Other Identifying Number Assigned by Agency:**
  FA2386-20-1-4086
- **Project Title:**
  Obtaining critical phase information for the design of refractory high-entropy superalloys
- **Project Director/Principal Investigator (PD/PI) Name, Title and Contact Information (e-mail address and phone number):**
  Ming-Hung, Tsai, Associate Professor, email: mhtsai@nchu.edu.tw,
  tel: +886-4-22840500 ext: 303
- **Name of Submitting Official, Title, and Contact Information (e-mail address and phonenumber), if other than PD/PI**
  Same as PI
- **Submission Date**
  06/29/2022
- **DUNS and EIN Numbers**
  DUNS: 656455102/EIN: 44-4444444
- **Recipient Organization (Name and Address)**
  National Chung Hsing University/ 145, Hsingda Rd., South Dist., Taichung City 40227 Taiwan
- **Recipient Identifying Number or Account Number, if any**
  401-30-099556
- **Project/Grant Period (Start Date, End Date)**
  09/30/2020, 03/29/2022
- **Reporting Period End Date**
  06/29/2022
- **Report Term or Frequency (annual, semi-annual, quarterly, other)**
  Annual report
- **Final Report? Select Yes or No**
  Yes
- **Signature of Submitting Official (signature shall be submitted in accordance with agency-specific instructions)**

DISTRIBUTION A: Distribution approved for public release.

Accomplishments

- **What were the major goals and objectives of this project?**

Statement of Objectives

- Investigate the equilibrium microstructure, phase constituents, and composition of phases in selected alloys around the B2 phase region of a model RHESA system and its B2-containing ternary subsystems.
- Obtain the partial ternary/pseudo-ternary phase diagrams around the B2 phase region at different temperatures in the RHESA and its ternary subsystems.
- Determine the B2 phase region at different temperature and its temperature range of stability in each system.
- Examine the existence of BCC+B2 phase region in each system.
- Investigate the reaction pathway responsible for forming the BCC+B2 microstructure in each system (if exist).
- Explore the relationship between the B2, BCC, BCC+B2 phase regions in the ternary systems and that in the pseudo-ternary (quinary) system.

Approach or Research Effort

- The RHESA system will be selected so that there is least number of B2-containing ternary subsystems, and the most existing phase data is available. This allows easy assessment of the RHESA system.
- The exact alloy compositions to be annealed in each ternary/pseudo ternary system will be determined so that phase information around the suspected B2 phase region is unraveled without significant overlap with existing phase data. The alloys will be annealed at three different temperatures (tentatively 700, 1000 and 1300^{o}C) to reach thermodynamic equilibrium.
- Alloys will be preparation by vacuum arc melting. Prior to equilibrium annealing, some alloys may require homogenization or even hot forging. The samples will be encapsulated in quartz tubes during annealing for oxidation protection.
- The microstructure, phase constituents, and composition of phases in the equilibrium annealed alloys will be identified by a combination of XRD, SEM, TEM, and EDS techniques. As a result, partial phase diagrams around the B2 phase regions in the RHESA and its B2-containing subsystems will be developed.
- Based on the partial phase diagrams, the B2 phase region and its stable temperature range will be determined. The existence of BCC+B2 phase

region in each system will be examined and the reaction pathway leading to BCC+B2 will be investigated.

- The relationship between the B2/BCC/BCC+B2 regions in the ternary systems and that in the pseudo-ternary system (quinary) will be explored.

- **What was accomplished under these goals?**

Major activities

1. In this work, 14 alloys in two refractory high entropy alloy systems were investigated. The equilibrium microstructure, phase constituents, and compositions of phases of each alloy after prolonged annealing at three different temperatures were unraveled. The partial pseudo-ternary phase diagram of the two systems at three temperatures was depicted according to the compositions of phases. Based on the phase diagrams, the B2 phase regions were also evaluated.
2. The two alloy systems are the Ti-Zr-Al-Nb-Ta (called the NT series) and its subsystem Ti-Zr-Al-Nb (called the N series). 7 alloys were selected in each system. The first alloy was selected as the center point at the composition of $(Ti_{50}Zr_{50})_2AlY$ in the $(Ti_{50}Zr_{50})$-Al-Y pseudo-ternary phase diagram, which is the representative composition of B2. The other six alloys then were decided by surrounding the center point. The compositions of the seven alloys in the $(Ti_{50}Zr_{50})$-Al-Y pseudo-ternary phase diagram are shown in Fig. 1, which were numbered 0-6. The specific composition of the alloys and the designation are in Table 1.
3. Each alloy was prepared by vacuum arc melting. The as-cast alloys were subsequently annealed at three temperatures to reach thermodynamic equilibrium, including 1300°C for 500 h, 1000°C for 1000 h and, 700°C for 1500 h (homogenized at 1300°C for 24 h first). Crystal structures of alloys were analysis by an X-ray diffractometer (BRUKER-D8 Discover), and by electron backscatter diffraction (JOEL JSM-7800F SEM equipped with Oxford NordlysMax^3 EBSD instrument.) if necessary. Microstructure observations and composition analyses were conducted by a JOEL-5400 scanning electron microscope (SEM) with energy dispersive X-ray spectroscopy (EDS) capability. Thus, the microstructure, phase constituents and the composition of phases in each alloy were obtained. Take the 1000°C annealed N1 alloy for example. The XRD pattern, SEM images and the EDS composition of N1 alloy are shown in Fig. 2. According to the XRD pattern, the peaks corresponded to the BCC, σ-$AlNb_2$ (tP30-CrFe, SG No. 136) and Al_3Zr_5 (hP16-Mn_5Si_3, SG No. 193) phases. Based on the peak intensities, the σ phase would dominate in the alloy. The microstructure of N1 is dendritic structure. In the dendrite region, the light grey phase in the core surrounded by the dark grey phase.

The interdendrite is the dark phase. According to the EDS, the light grey dendrite core corresponded to the BCC phase. The dark grey phase around the core was richer in Nb and Al, which corresponded to the σ phase. The dark interdendrite was Al- and Zr-rich, which corresponded to the Al_3Zr_5 phase. Based on the above, the phase constituents, microstructure and phase compositions of N1 were obtained.

4. Microstructures of some alloys were still fine after 700°C annealing for 1500 h, and were difficult to analyze by SEM. Therefore, TEM was used to investigation their microstructures and phase composition. An example is shown in Fig. 3 (the NT0 alloy annealed at 700°C for 1500). The TEM image corresponded to the yellow rectangle in the SEM BEI image. The microstructure was extremely fine and complex. Three different phases were identified by TEM (marked A, B and C). They corresponded to Al_3Zr_5 (hP16- Mn_5Si_3, SG No. 193), BCC, and $AlTi_3$ (hP8-Mg_3Cd, SG No. 194) phases, respectively.

Specific objectives

1. Investigate the equilibrium microstructure, phase constituents, and composition of phases in selected alloys around the B2 phase region of Ti-Zr-Al-Nb-Ta system and its subsystem Ti-Zr-Al-Nb.
2. Obtain the partial ternary/pseudo-ternary phase diagrams around the B2 phase region at 700, 1000 and 1300°C in the Ti-Zr-Al-Nb-Ta system and its subsystem Ti-Zr-Al-Nb.
3. Examine the existence of BCC+B2 phase region in each system.
4. Determine the B2 phase region at different temperature and its temperature range of stability in each system.
5. Investigate the reaction pathway responsible for forming the BCC+B2 microstructure in each system (if exist).
6. Explore the relationship between the B2, BCC, BCC+B2 phase regions in the ternary systems and that in the pseudo-ternary (quinary) system.

Significant results

1. Identified the equilibrium phases, microstructure and composition of phases in each alloys at different temperatures

The equilibrium microstructure, phases and composition of phases of each alloy in N and NT series at the three temperatures were identified. This information is listed in Tables 2-7. The phases in N and NT series alloys are in general similar. According to the tables, the BCC phase was present in all the alloys regardless of the annealing temperature except for the N2 alloy at 1000 and 700°C. However, no stable B2 phase

DISTRIBUTION A: Distribution approved for public release.

was observed in the two systems from 700-1300°C. The σ phase and various types of Al-Zr intermetallic phases were also prevalent in the alloys.

2. The interconnected structure in the quenched alloy and the original structure at high-temperature

Our primary goal is to investigate the existence of the B2 phase and the BCC + B2 phase region in N and NT series alloys in equilibrium conditions. Thus, the identification of the BCC and the B2 phases is of great importance. The identification of these phases, however, turned out to be challenging in these alloys. The BCC or B2 phases as identified by SEM and XRD were not really a single phase when examined with TEM. Instead, a special and complex kind of nanostructure was found in these phases. The 1300°C-annealed N4 alloy is good example (Fig. 4). The XRD pattern and SEM micrographs both suggested that this alloys were a single-phase BCC alloy. However, TEM observations showed that this alloy had a nanoscale interconnected structure (Fig. 5). The wavelength of the structure was on the order of 10-20 nm. As a result, 1300°C N4 is not really a single phase alloy. Interestingly, the selected area diffraction pattern (SADP) of the alloy (Fig. 5 (b)) revealed a BCC single phase pattern, with extremely weak B2 superlattice spots. The dark-field (DF) images corresponding to the superlattice spot (red circle) also showed extremely weak contrast (Fig. 5 (b)). In fact, the interconnected microstructure was widely observed within the BCC/B2 phases in the alloys regardless of compositions and annealing temperature. All the interconnected microstructure had similar wavelengths (see Fig. 6 for three other examples).

The nanoscale wavelength suggested that these microstructures were not the equilibrium microstructure during annealing, they were more likely formed during the quenching process. The fast reaction rate and the identical crystal structure in the two separated phases suggests that the interconnected structure is a result of spinodal decomposition. Similar microstructures were observed in other studies [1-5]. It was proposed that the interconnected microstructure might be due to the phase separation from a single phase BCC via spinodal decomposition during cooling [1, 2, 4, 6]. It is also suggested that the two-phase separation in RHESAs is mainly due to the miscibility gap of Ta-Zr [7-9]. However, spinodal decomposition would only produce the same crystal structure from the parent BCC/B2 phase. Thus, an additional ordering or disordering process must occur. It has been proposed that some two-phase alloys undergo a two-step decomposition process consisting of an ordering transition followed by spinodal decomposition [10]. Therefore, the formation of the BCC + B2 interconnected structure is more possibly from a high-temperature BCC phase, which spinodally decomposes into two BCC phases of different compositions, followed by B2

DISTRIBUTION A: Distribution approved for public release.

ordering within one of the phase-separated regions.

In summary, the interconnected structure widely formed in the N and NT series alloys regardless of annealing temperatures. As mentioned above, the observation of BCC + B2 interconnected structure actually suggested an original high-temperature BCC phase, which spinodally decomposes into two BCC phases of different compositions, and one of the phases could subsequently go through B2 ordering.

3. Does the B2 phase exist in the N and NT series alloys?

Based on the above investigations, we conclude that no equilibrium B2 phase existed in the N and NT series alloys at 700-1300°C. All the phases that seems to be a BCC/ B2 phase actually contained the interconnected structure when observed by TEM. Thus, the B2-ordering observed in the sample quenched from 700, 1000, or 1300°C was not really due to the formation of B2 phase at these temperatures. Instead, the ordering probably took place during quenching. In the quenching process, a BCC phase first went through spinodal decomposition. Then ordering took place in one of the BCC phases subsequently. Thus, no equilibrium B2 phase was confirmed in the N and NT series alloys at 700-1300°C. Since our composition design was centered around the most possible B2 composition X_2AlY, the fact that these seven alloys did not contain equilibrium B2 phases suggests that the absence of B2 phase is probably true for all the whole Ti-Zr-Al-Nb-Ta and Ti-Zr-Al-Nb alloy systems, not just for the seven alloys.

Compared to other studies, some RHESAs with similar compositions to the NT4 and NT5 were reported to have the B2 phase. [2-4, 11-13]. However, most of them were far from thermodynamic equilibrium (annealed at 600-800°C for 1-120 h). On the other hand, other RHESAs after prolonged annealing were also reported to have the B2 phase [14, 15], which were probably caused from the interconnected structure as mentioned before. Thus, so far no solid evidence that the equilibrium B2 phase is formed in Ti-Zr-Al-Nb-Ta systems.

4. Phases and the approximate phase regions in N and NT series at different temperatures (in pseudo ternary phase diagram)

According to the EDS composition in Tables 2-7, the phases in the N and NT alloys at 700, 1000, and 1300°C can be plotted in the X-Al-Y pseudo-ternary phase diagrams. These were shown in Figs. 7 and 8. As a result, the preliminary phase regions of related phases in the N and NT alloys were also suggested and depicted in the pseudo-ternary phase diagram shown in Figs. 9 and 10. The overall trend of N and NT series alloys are discussed as follow:

N series

DISTRIBUTION A: Distribution approved for public release.

Seven types of phases occurred in the N series alloys at 700-1300°C annealing including BCC, σ, Al_3Zr_4 (hP7-Al_3Zr_4, SG No. 191), Al_3Zr_5, Laves C14-Al_2Zr (hP12-$MgZn_2$, SG No.194), ω-$AlZr_2$ (hP6-$Co_{1.75}Ge$, SG No. 194) and $AlTi_3$ phases (Tables 2-4). All phases in N series belonged to the intermetallic (IM) phase except for the BCC phase. In addition, these IM phases were related to the binary IM phases of Al. In particular, four of them were related to the binary Al-Zr phases, which suggested the Al-Zr pair was dominant in the N series. According to the Tables 2-4, the composition of IM phases was mainly based on their binary parent phases with other solid solute elements. For example, the Al_3Zr_5 phase was consist of 75% Al and Zr (Zr is more than Al) with partial Nb and Ti. It seems that these IM phases highly inherited not only the structure but also the composition from their subsystems. The composition of the only solid solution in N series BCC phases could vary over a wide span.

The compositions of phases in the N series alloys after 700-1300ºC annealing were plotted in the pseudo-ternary phase diagrams (Fig. 7) to compare the phase formation behaviors at different temperatures. The N series alloys at 1300 and 1000°C contained four types of phases, which were quite similar (only one of the four phases was different). Compared to the 1300 and 1000°C annealing, the N series alloys at 700°C were more complex, which contained all seven phases. Among all phases, the BCC, σ and Al_3Zr_5 phases were formed in N series at 700-1300°C, suggesting that they were the most stable phases in this system. The composition of the same type of the IM phases in different alloys or at different temperatures did not change significantly. However, the composition of the BCC phases changed substantially especially at 700°C. It can be noted that the composition distribution of the BCC phases in the 700°C phase diagram suddenly reached toward the right bottom side. In fact, the varied distribution of the B2 phases at 700°C was due to the second B2 phase formation in N1 and N6 alloys – the two BCC phases at the right bottom side were the compositions of the new-formed BCC phases.

Based on Fig. 7, the location of each phase region can be roughly inferred, which was shown in Fig. 9. As mentioned above, all IM phases were related to Al except for the BCC phase. Besides, the composition of IM phases was mainly composed of their binary pairs of their parent phases with other solid solute elements. Therefore, the IM phase regions should extend from the side of their binary parent phases inward the phase diagrams. For example, the Al_3Zr_5 phase region was supposed to extend from the binary stoichiometry of Al_3Zr_5 to near the compositions of the phases. The other Al-Zr phase regions (Al_3Zr_4, C14 and ω) also extended from their binary stoichiometry of compound to their compositions. The only binary σ phase in the quaternary N series was $AlNb_2$. They were indeed richer in Al and Nb in the N series. Thus, the σ phase region was supposed to extend from the $AlNb_2$. Similarly, the $AlTi_3$ phase region was

DISTRIBUTION A: Distribution approved for public release.

also extend from the Ti-Al side. The same IM phase regions at 700-1300°C were quite similar. While they were slightly extensive at 700°C.

As for the BCC phase regions, they basically extended from the X-Nb side toward the center of the phase diagrams and changed with annealing temperatures. The BCC phase region at 1300°C extended to a really wide range of Al~40 at.% . On the contrary, the BCC regions at 1000°C and 700°C were quite similar. It is noted that the aforementioned two BCC phases in the 700°C -annealed N1 and N6 alloys are due to the interaction of individual elements in Ti-Zr-Al-Nb system. In the system, only binary Nb-Zr has a miscibility gap [16], which occurs at 977°C (Fig. 11(a)). When inside the miscibility gap, a single phase spontaneously separates into two phases with an identical crystal structure but different compositions. The compositions of the two separating phases lied on the opposite sides of the gap boundary are solute-rich and solute-lean. In fact, the two BCC phases in the 700-annealed N1 and N6 alloys were Nb-rich and Nb-lean BCC phases, respectively. This suggested that the two alloys experienced phase separation due to the miscibility gap between Nb and Zr. According to the locations of the two BCC phases in N1 and N6 alloys, the miscibility gap in N series at 700°C was roughly depicted (black dotted lines).

It should be noted that although the pseudo-ternary phase diagrams are very convenient tools to quickly understand the system and are conventionally used. They are actually a projection of the real, higher-order diagram. This leads to clear differences from ordinary ternary phase diagrams. For example, the pseudo-ternary phase diagrams of the N series are a projection of the quaternary phase diagram on to the $Ti_{50}Zr_{50}$-Al-Nb planes (Fig. 12). Thus, the exact contents of Ti and Zr cannot be reflected on the Ti-Zr axis, and the composition points or phase regions are actually somewhere above or below the plane of the paper. This leads to weird configurations in the diagram, such as overlapping single phase regions.

NT series

Seven types of phases occurred in the NT series alloys at 700-1300°C annealing including BCC, σ, Al_3Zr_4 (hP7-Al_3Zr_4, SG No. 191), Al_3Zr_5, Laves C14-Al_2Zr (hP12-$MgZn_2$, SG No.194), ω-$AlZr_2$ (hP6-$Co_{1.75}Ge$, SG No. 194) and $AlTi_3$ phases, which were shown in Tables 5-7. The types of phases were identical with the N series, which suggesting that Ta addition did not affect the phase types. All phases in NT series belong to the IM phase. except for the BCC phase. Moreover, these IM phases were related to the binary IM phases of Al. In particular, four of them were related to the binary Al-Zr phases, suggesting that the Al-Zr pair was also dominant in the NT series alloys. According to the Table 5-7, the compositions of IM phases were mainly based on their binary parent phases and other solid solute elements. It seems that these IM phases

DISTRIBUTION A: Distribution approved for public release.

highly inherited the structure and the composition from their subsystems. On the contrary, the compositions of the only solid solution in NT series BCC phases could vary over a wide span.

The compositions of phases in the N series alloys after 700-1300ºC annealing were plotted in the pseudo-ternary phase diagrams (Fig. 8) to compare the phase formation behaviors at different temperatures. The NT series alloys at 1300 and 1000°C contained four and five phases, respectively. Four of them were identical in both annealing conditions. Compared to the 1300 and 1000°C annealing, the NT series alloys at 700°C were more complex, which contained all seven phases. Among all phases, the BCC, σ and Al_3Zr_5 phases were formed at 700-1300°C, suggesting that they were the most stable phases in this system. The composition of the same type of IM phases in different alloys or at different temperatures did not change significantly. However, the composition of the BCC phases changed substantially The composition distribution of the BCC phases shifted to the right bottom side with the decreasing temperature. In particular, the compositions of the BCC phases at 700°C were almost located on the X-Y axis which was near the binary XY. In fact, the varied distribution of the B2 phases at 700°C was due to the second B2 phase formation in the four alloys (NT1, NT4, NT5 and NT6) – the BCC phases at the right bottom side were the compositions of the new-formed BCC phases. This trend was similar to that in the N series.

Based on Fig. 8, the location of each phase region can be roughly inferred, which was shown in Fig. 10. As mentioned above, all IM phases were related to the Al. Besides, they were mainly composed of their binary pairs of the parent phases and the other solid solute elements. Therefore, the IM phase regions should extend from the side of their binary parent phases inward the phase diagrams. For example, the region of the Al_3Zr_5 phases was supposed to extend from the binary stoichiometry of Al_3Zr_5 near to the compositions of the phases. The other Al-Zr phase regions (Al_3Zr_4, C14 and ω) also extended from their binary stoichiometry of compounds to their actual compositions. The binary σ phase in the quinary NT system were $AlNb_2$ and $AlTa_2$. These σ phases were indeed richer in Al, Nb and Ta. Thus, the σ phase region should extend from the stoichiometry of $Al(Nb, Ta)_2$. Similarly, the $AlTi_3$ phase region extended from the Ti-Al side. The regions of the same IM phase at 700-1300°C were quite similar. They were slightly extensive at 700°C except for the σ phase region.

As for the BCC phase regions, they extended from the X-Nb side toward the center of the phase diagrams and extended to a really wide range of Al~40 at.% at the three temperatures. It is noted that the aforementioned two BCC phases at 1000 and 700°C were resulted from the miscibility gap in Ti-Zr-Al-Nb-Ta system. In NT seires, both Nb-Zr and Ta-Zr have a miscibility gap (Fig. 11), which occurs at 977°C and 1783°C, respectively. Compared to the N system, the phase separation was observed at higher

DISTRIBUTION A: Distribution approved for public release.

temperature in NT series alloys due to the higher temperature of Ta-Zr miscibility gap. According to the compositions of these two BCC phases in the alloys, the miscibility gaps in NT series at 1000 and 700°C were depicted (black dotted lines) in Fig. 10. It seems that the miscibility gap was extensive with the decreasing temperatures.

Comparisons between the N and NT series

In general, the phase types in the two series (N and NT series) are identical. Only a few differences were observed between the two series at different temperatures, e.g. the Laves phase was formed in the NT series but not in the N series at 1000°C. Thus, Ta addition did not affect the phase types. In contrast, Ta addition led to the different phase formation behavior between the two series. Specifically, Ta addition increased the higher temperature of the miscibility gaps, which led to the phase separation at higher temperature in the NT series than the N series.

The distributions of phases were quite similar in pseudo ternary phase diagrams of the two series except for the BCC phases. The same IM phases were located on the similar site in both series, which lead to the similar IM phase fields in both series. However, the BCC phase fields in the two series were very different. The BCC phase field in NT series reached from the X-Y side to the range of Al~40% at all temperatures, while such a wide phase field only occurred in N series at 700°C.

DISTRIBUTION A: Distribution approved for public release.

(TiZr)-Al-Y pseudo-ternary phase diagram

Number	Alloy
0	$(TiZr)_{50}Al_{25}Y_{25}$
1	$(TiZr)_{35}Al_{25}Y_{40}$
2	$(TiZr)_{42.5}Al_{40}Y_{17.5}$
3	$(TiZr)_{65}Al_{25}Y_{10}$
4	$(TiZr)_{65}Al_{10}Y_{25}$
5	$(TiZr)_{50}Al_{10}Y_{40}$
6	$(TiZr)_{40}Al_{20}Y_{40}$

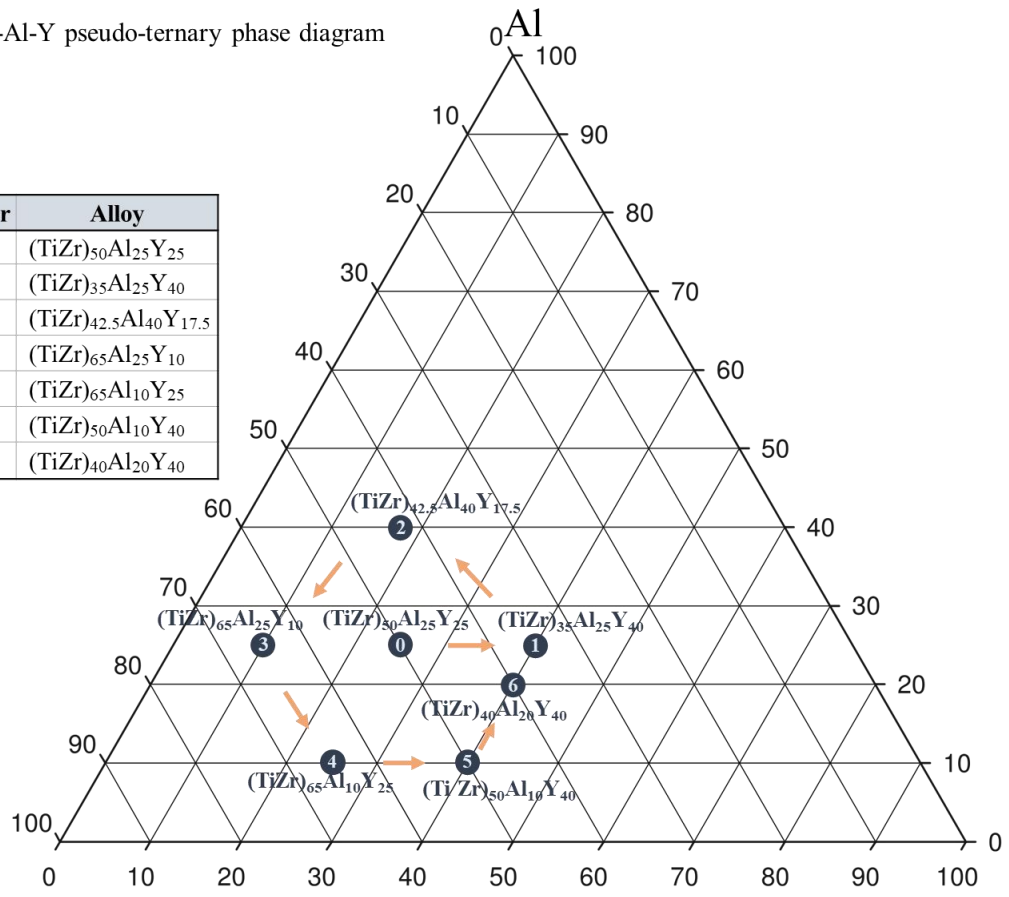

Fig. 1 (TiZr)-Al-Y pseudo-ternary phase diagram. The alloys were numbered according to their composition on the pseudo-ternary phase diagram.

N1 – $(TiZr)_{35}Al_{25}Nb_{40}$ annealed at 1000ºC for 1000 h

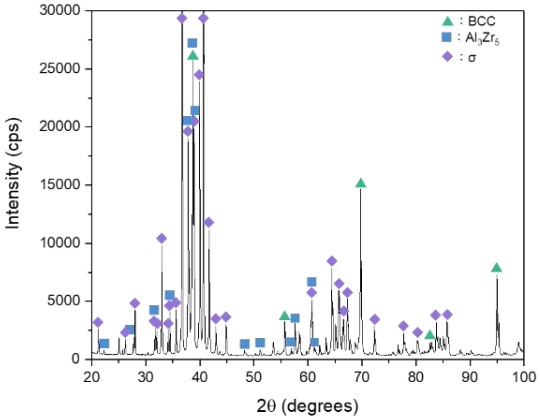

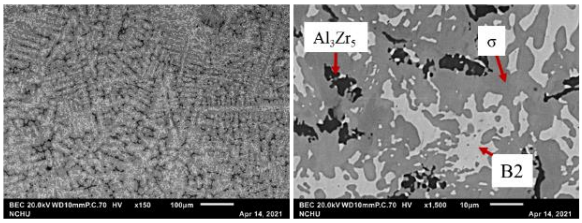

Alloy	Nominal Composition	Region/Phase	Composition (at.%)				Vol.
			Ti	Zr	Al	Nb	(%)
N1	$(TiZr)_{35}Al_{25}Nb_{40}$	overall	17.2	17.8	23.7	41.3	N/A
		BCC	25.6	11.6	10.8	52.0	45
		sigma	15.4	18.1	27.5	39.1	50
		Al_3Zr_5	9.7	40.0	35.3	15.0	5

Fig. 2 Phase constituents, microstructure and the composition of phases of the N1 alloy after 1000°C annealing for 1000 h

DISTRIBUTION A: Distribution approved for public release.

NT0 - $(TiZr)_{50}Al_{25}(NbTa)_{25}$ annealed at 700ºC for 1500 h

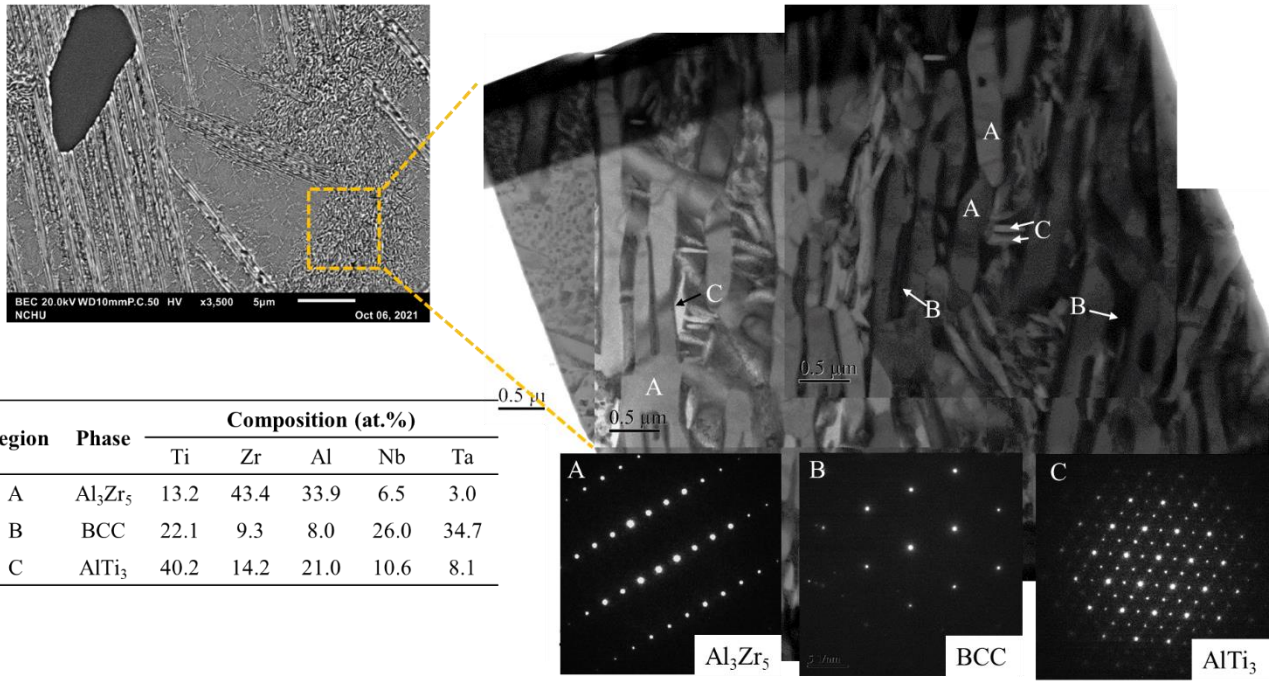

Region	Phase	Composition (at.%)				
		Ti	Zr	Al	Nb	Ta
A	Al_3Zr_5	13.2	43.4	33.9	6.5	3.0
B	BCC	22.1	9.3	8.0	26.0	34.7
C	$AlTi_3$	40.2	14.2	21.0	10.6	8.1

Fig.3 Very fine structure in NT1 alloy after 700°C annealing for 1500 h. The phases are identified by TEM.

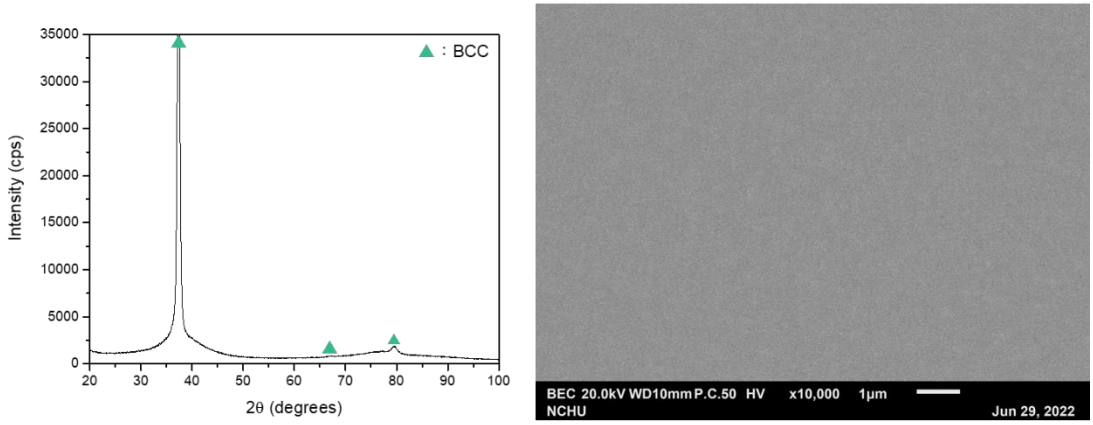

Fig. 4 The XRD pattern and the SEM image suggest that the N4 alloy had a single phase BCC structure after 1300°C annealing

DISTRIBUTION A: Distribution approved for public release.

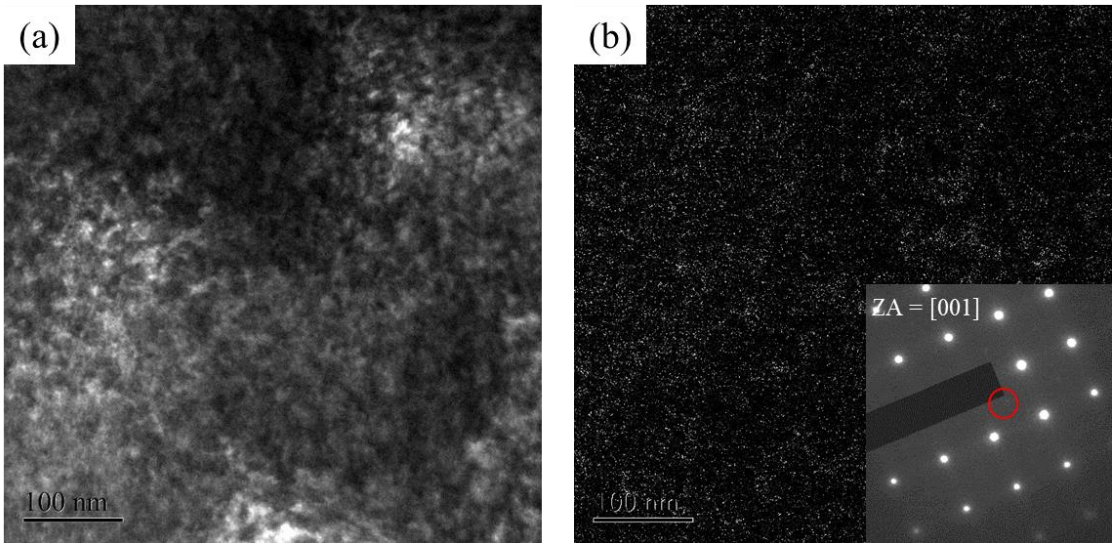

Fig. 5 TEM images of the N4 alloy after 1300°C annealing. (a) Bight field image; (b) Dark field image based on the red circle in the SADP of the [001]-zone axis.

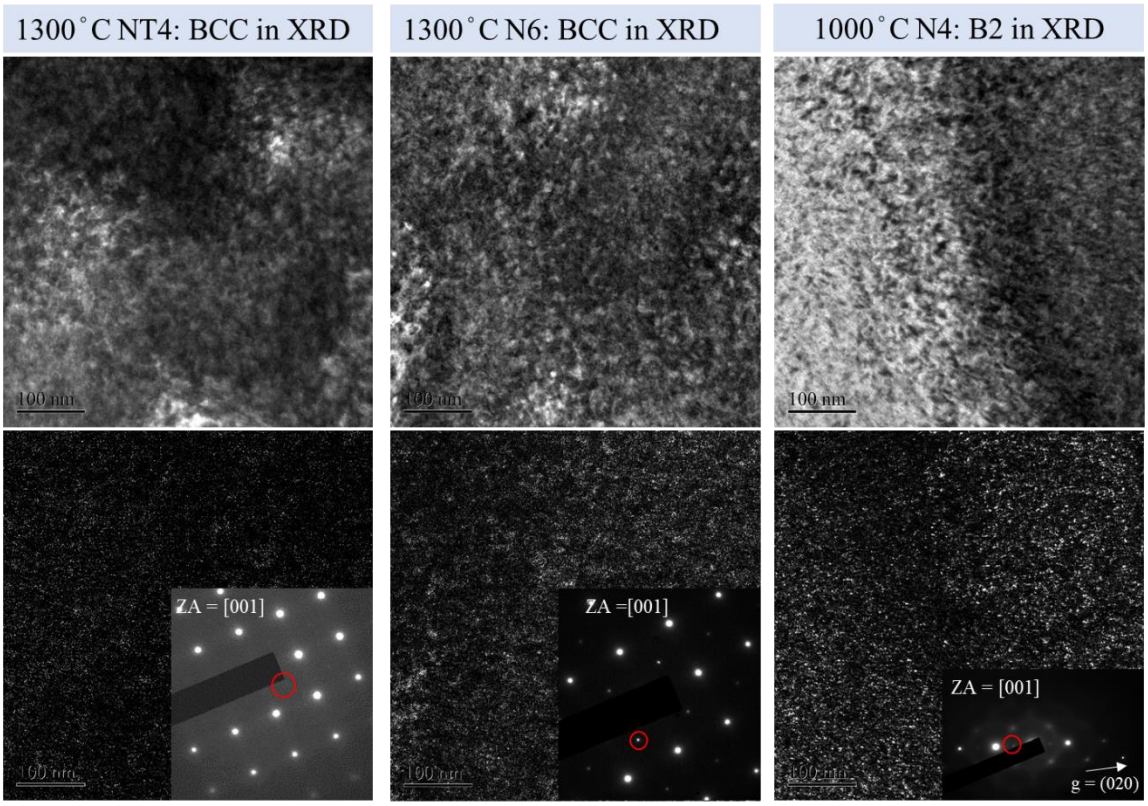

Fig. 6 The interconnected structure observed in different alloys

DISTRIBUTION A: Distribution approved for public release.

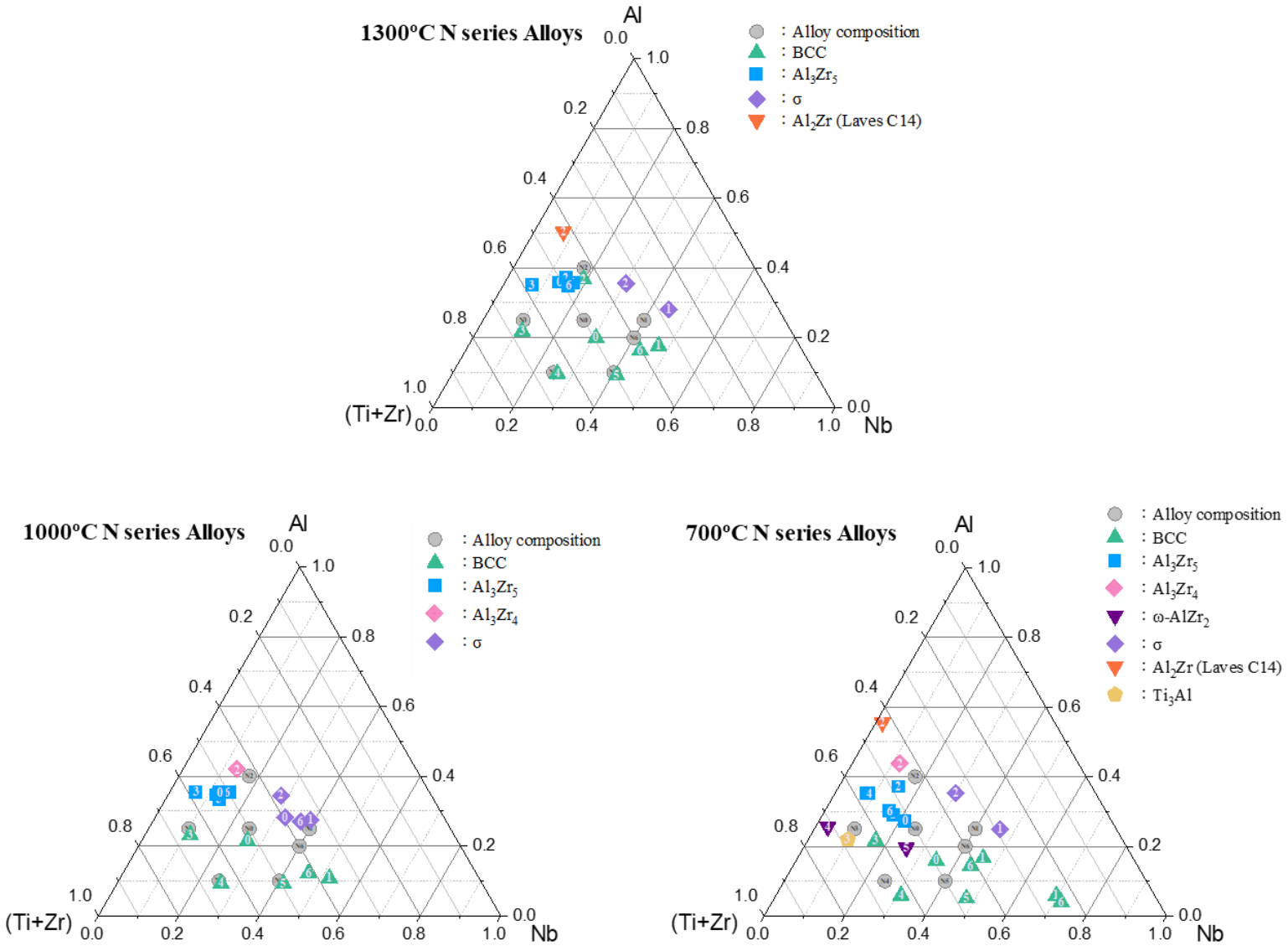

Fig. 7 Composition of phases in the N series alloys after 700-1300ºC annealing as plotted in the pseudo-ternary phase diagram, where Ti and Zr are viewed as a pseudo element.

DISTRIBUTION A: Distribution approved for public release.

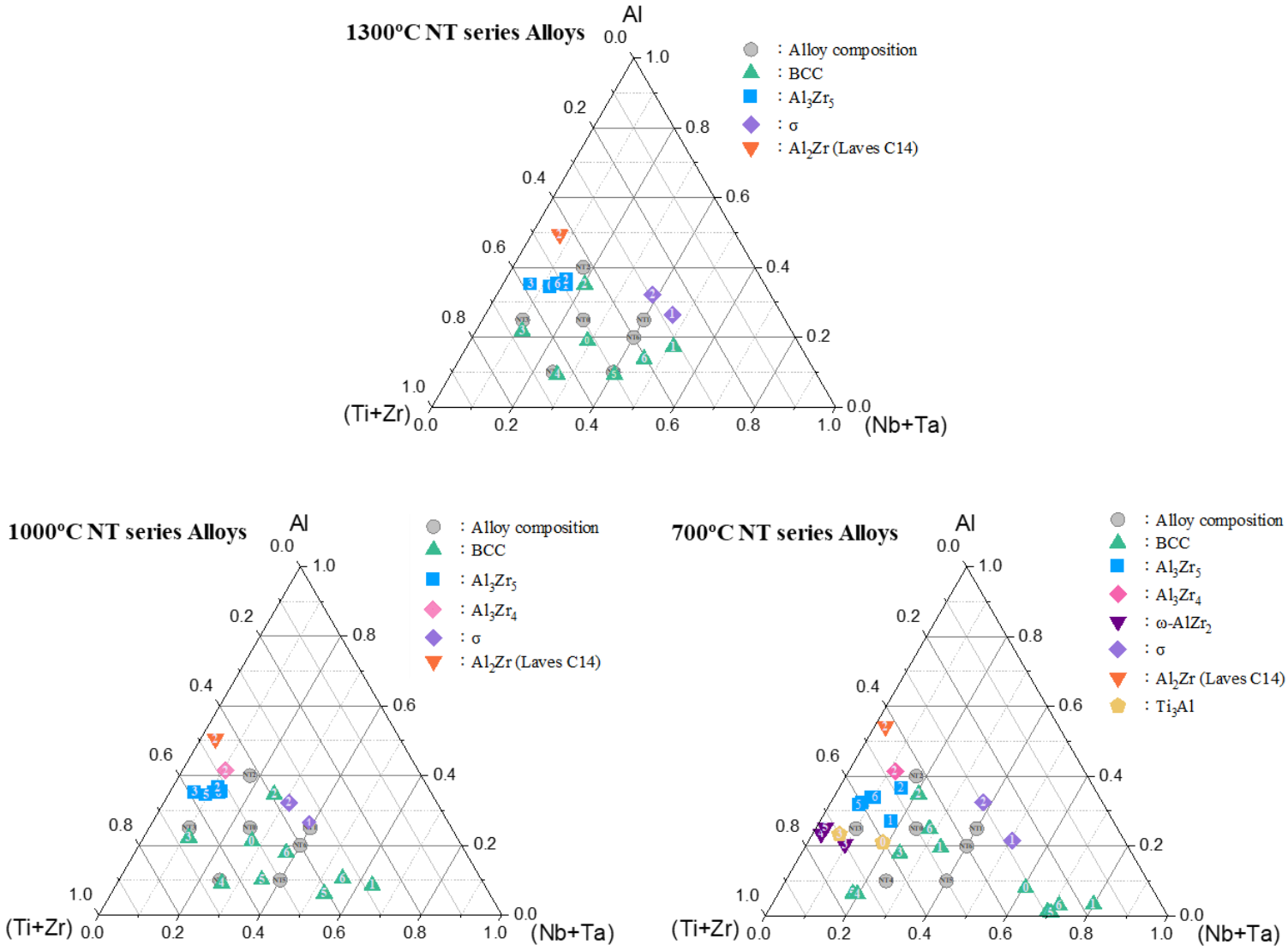

Fig. 8 Composition of phases in the NT series alloys after 700-1300ºC annealing as plotted in the pseudo-ternary phase diagram, where Ti and Zr, Nb and Ta are viewed as two pseudo elements.

DISTRIBUTION A: Distribution approved for public release.

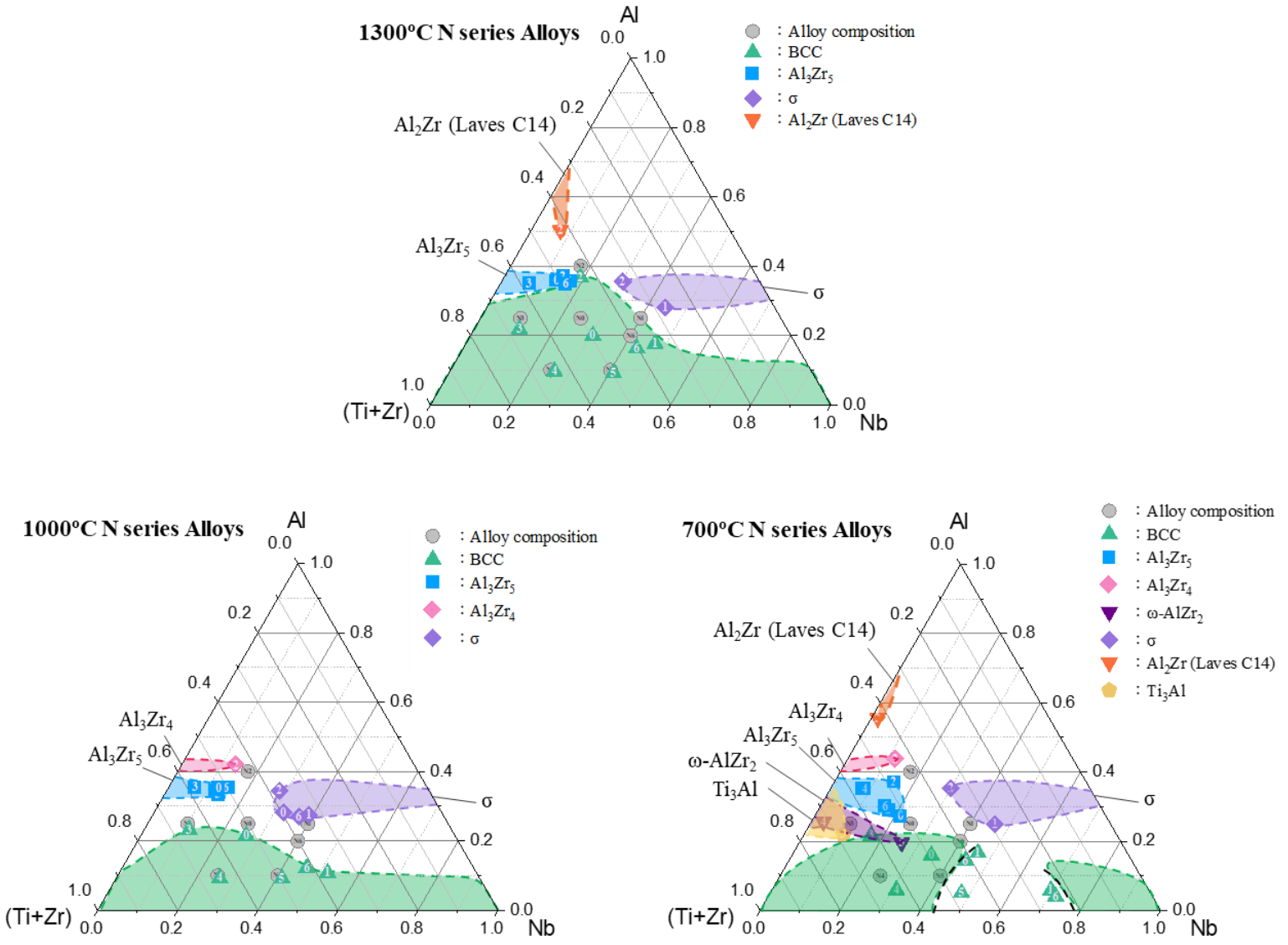

Fig. 9 Approximate phase regions in the Ti-Zr-Al-Nb system (N series) in pseudo-ternary phase diagram at 700, 1000, and 1300ºC (Ti and Zr are regarded as one pseudo element) 其他你改

DISTRIBUTION A: Distribution approved for public release.

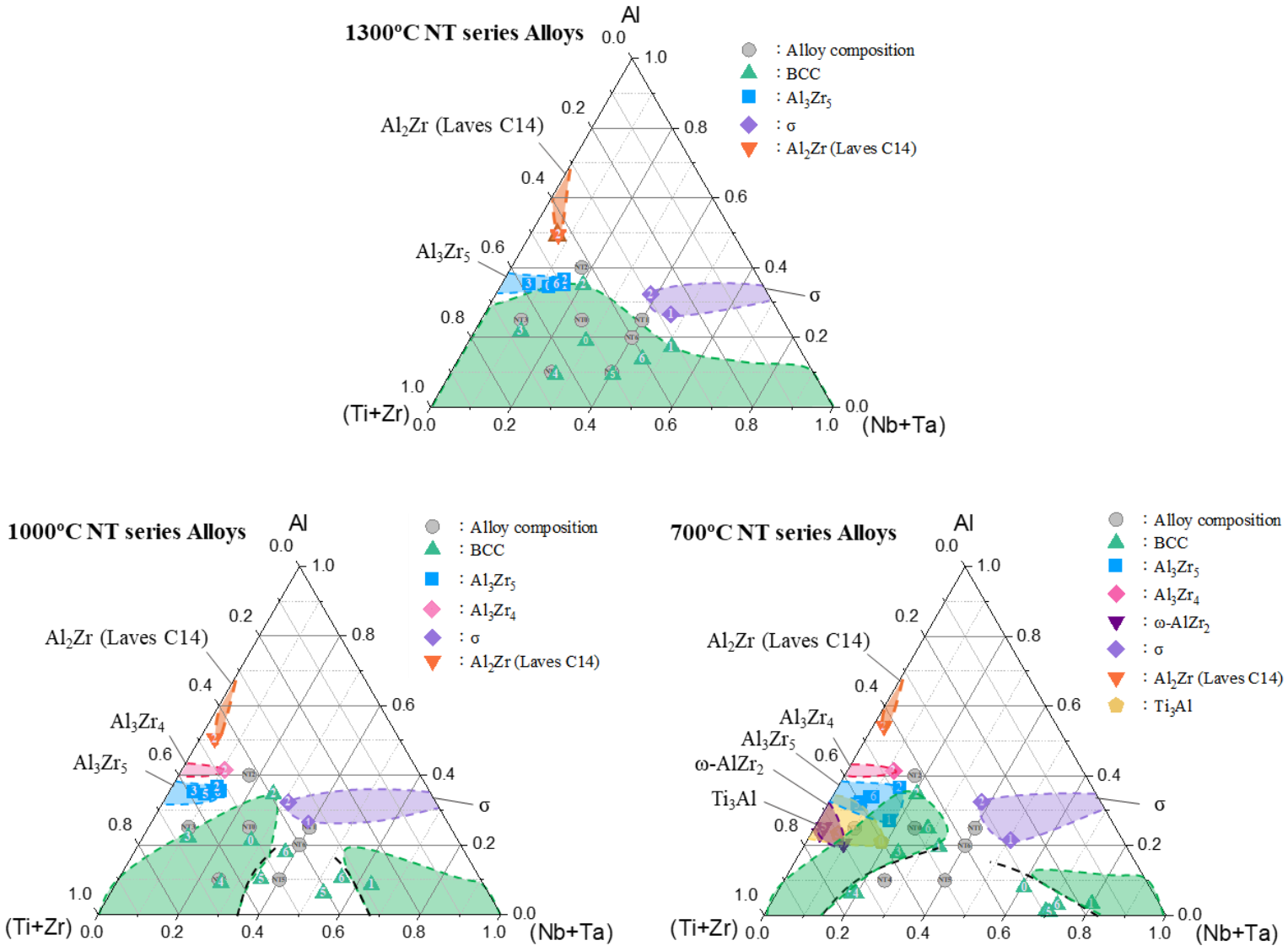

Fig. 10 Approximate phase regions of NT series at 700-1300ºC annealing in pseudo-ternary phase diagram, where Ti and Zr, Nb and Ta are viewed as two pseudo elements.

DISTRIBUTION A: Distribution approved for public release.

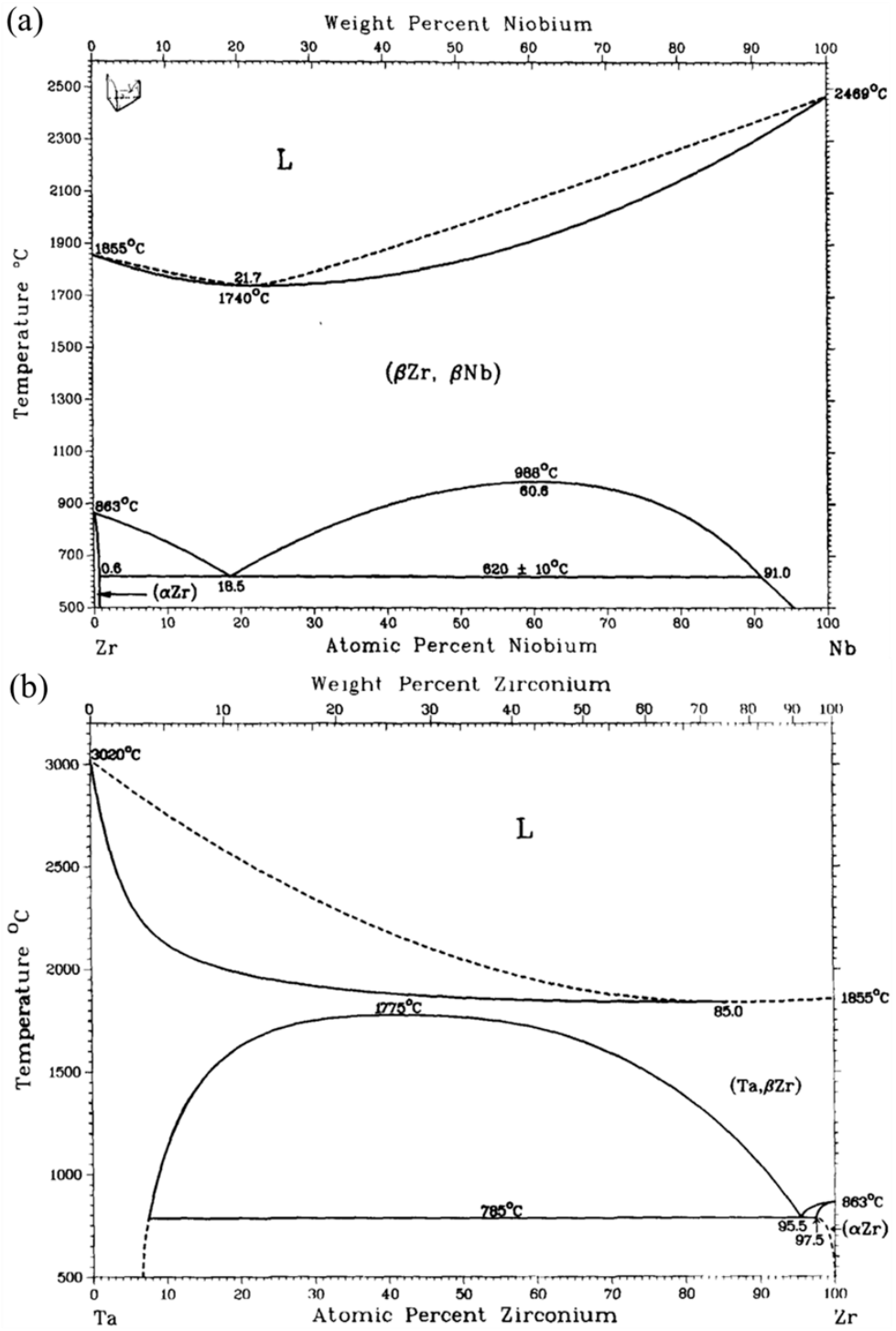

Fig. 11 Binary phase diagrams of (a) Zr-Nb and (b) Zr-Ta [16]

DISTRIBUTION A: Distribution approved for public release.

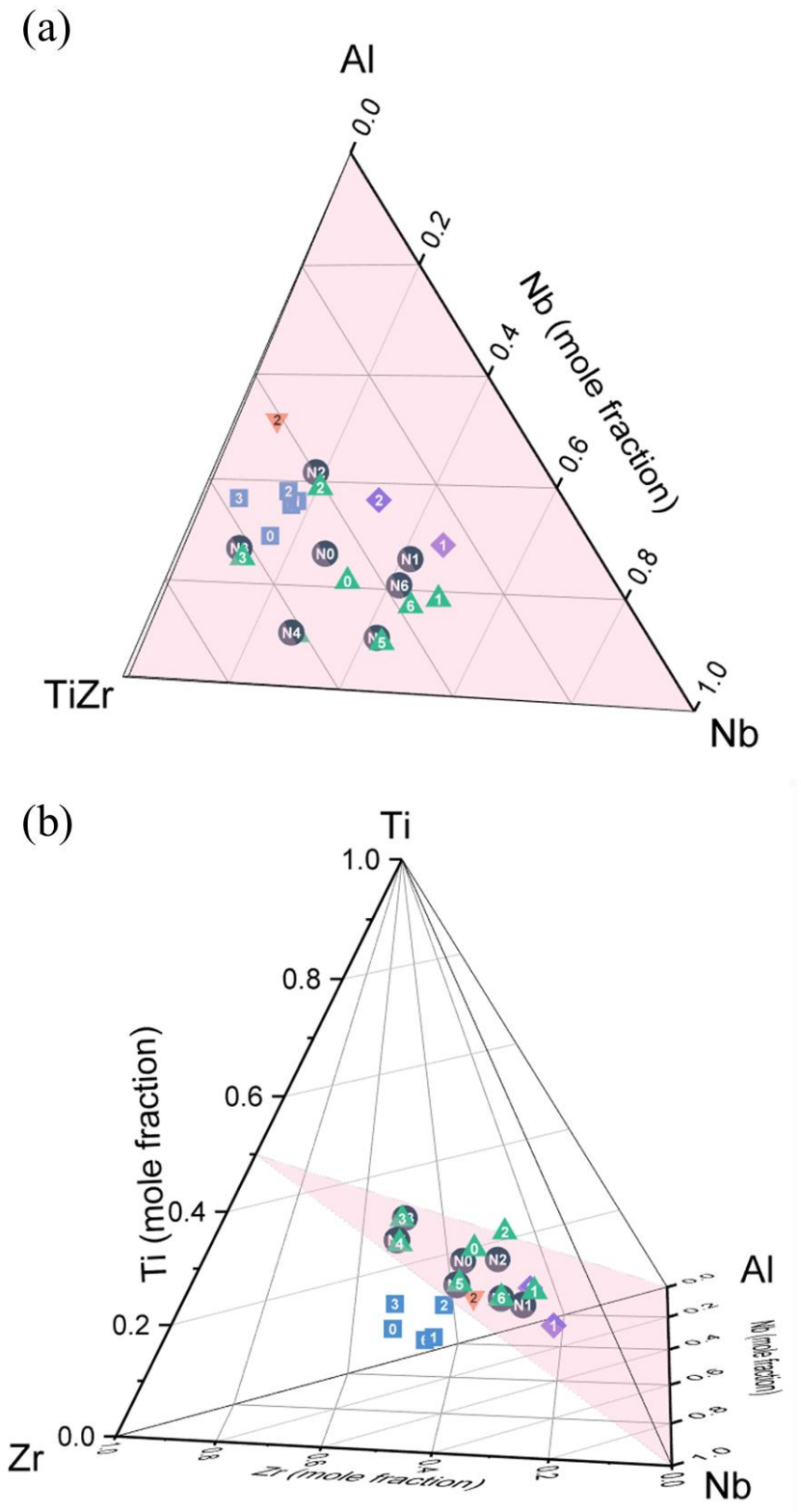

Fig. 12 (a) The pseudo ternary phase diagram of 1300°C-annealed N series alloys is a projection of the quaternary phase diagram on to the $Ti_{50}Zr_{50}$-Al-Nb plane (colored pink) (b) The actual positions of the phases in the quaternary phase diagram.

DISTRIBUTION A: Distribution approved for public release.

Table 1 List of alloys in the present work
(along with their designations and compositions)

NT-Series						N-Series				
Alloy Designation/ Chemical Formula	**Nominal composition (at.%)**					**Alloy Designation/ Chemical Formula**	**Nominal composition (at.%)**			
	Ti	Zr	Al	**Nb**	**Ta**		Ti	Zr	Al	**Nb**
NT0 $(TiZr)_{50}Al_{25}(NbTa)_{25}$	25.0	25.0	25.0	**12.5**	**12.5**	**N0** $(TiZr)_{50}Al_{25}Nb_{25}$	25.0	25.0	25.0	**25.0**
NT1 $(TiZr)_{35}Al_{25}(NbTa)_{40}$	17.5	17.5	25.0	**20.0**	**20.0**	**N1** $(TiZr)_{35}Al_{25}Nb_{40}$	17.5	17.5	25.0	**40.0**
NT2 $(TiZr)_{42.5}Al_{40}(NbTa)_{17.5}$	21.25	21.25	40.00	**8.75**	**8.75**	**N2** $(TiZr)_{42.5}Al_{40}Nb_{17.5}$	21.25	21.25	40.00	**17.50**
NT3 $(TiZr)_{65}Al_{25}(NbTa)_{10}$	32.5	32.5	25.0	**5.0**	**5.0**	**N3** $(TiZr)_{65}Al_{25}Nb_{10}$	32.5	32.5	25.0	**10.0**
NT4 $(TiZr)_{65}Al_{10}(NbTa)_{25}$	32.5	32.5	10.0	**12.5**	**12.5**	**N4** $(TiZr)_{65}Al_{10}Nb_{25}$	32.5	32.5	10.0	**25.0**
NT5 $(TiZr)_{50}Al_{10}(NbTa)_{40}$	25.0	25.0	10.0	**20.0**	**20.0**	**N5** $(TiZr)_{50}Al_{10}Nb_{40}$	25.0	25.0	10.0	**40.0**
NT6 $(TiZr)_{40}Al_{20}(NbTa)_{40}$	20.0	20.0	20.0	**20.0**	**20.0**	**N6** $(TiZr)_{40}Al_{20}Nb_{40}$	20.0	20.0	20.0	**40.0**

Table 2 Phase constituents and composition of phases in the N series alloys after 1300°C annealing for 500 h

Alloy	**Nominal Composition**	**Region/Phase**	**Overall/Phase Composition (at.%)**			
			Ti	**Zr**	**Al**	**Nb**
N0	$(Ti,Zr)_{50}Al_{25}Nb_{25}$	overall	25.0	25.0	23.7	26.3
		BCC	28.5	21.0	20.0	30.6
		Al_3Zr_5	10.6	40.1	35.8	13.5
N1	$(Ti,Zr)_{35}Al_{25}Nb_{40}$	overall	17.0	18.2	23.6	41.2
		BCC	21.9	13.1	17.7	47.2
		σ	13.2	14.1	28.0	44.6
		Al_3Zr_5	8.4	38.9	35.6	17.1

DISTRIBUTION A: Distribution approved for public release.

N2	$(Ti,Zr)_{42.5}Al_{40}Nb_{17.5}$	overall	21.6	21.1	39.0	18.3
		BCC	27.0	17.1	36.8	19.1
		Al_3Zr_5	13.8	34.6	37.0	14.6
		σ	17.5	16.7	35.6	30.3
		Laves C14	11.4	31.0	50.3	7.3
N3	$(Ti,Zr)_{65}Al_{25}Nb_{10}$	overall	32.4	33.1	23.5	11.1
		BCC	32.8	32.7	23.3	11.2
		Al_3Zr_5	14.3	43.7	35.4	6.6
N4	$(Ti,Zr)_{65}Al_{10}Nb_{25}$	single phase BCC	32.0	32.2	9.7	26.1
N5	$(Ti,Zr)_{50}Al_{10}Nb_{40}$	single phase BCC	25.4	24.3	9.2	41.1
N6	$(Ti,Zr)_{40}Al_{20}Nb_{40}$	overall	19.7	21.3	18.4	40.7
		BCC	21.1	19.2	16.3	43.3
		Al_3Zr_5	8.1	40.7	34.9	16.4

Table 3 Phase constituents and composition of phases in N alloys after 1000°C annealing for 1000 h

Alloy	**Nominal Composition**	**Region/Phase**	**Composition (at.%)**			
			Ti	**Zr**	**Al**	**Nb**
N0	$(TiZr)_{50}Al_{25}Nb_{25}$	overall	25.8	24.8	23.4	26.1
		BCC	28.2	24.0	21.5	26.3
		σ	17.7	21.8	28.2	32.3
		Al_3Zr_5	11.3	40.9	35.3	12.5
N1	$(TiZr)_{35}Al_{25}Nb_{40}$	overall	17.2	17.8	23.7	41.3
		BCC	25.6	11.6	10.8	52.0
		σ	15.4	18.1	27.5	39.1
		Al_3Zr_5	9.7	40.0	35.3	15.0
N2	$(TiZr)_{42.5}Al_{40}Nb_{17.5}$	overall	21.6	21.7	37.9	18.8
		Al_3Zr_4	17.8	27.9	40.5	13.9
		σ	13.1	35.5	36.2	15.3
		Al_3Zr_5	25.6	14.8	35.9	23.8
N3	$(TiZr)_{65}Al_{25}Nb_{10}$	overall	32.4	33.1	23.5	11.0
		BCC	32.8	32.7	23.3	11.2

DISTRIBUTION A: Distribution approved for public release.

		Al_3Zr_5	14.3	43.7	35.4	6.6
N4	$(TiZr)_{65}Al_{10}Nb_{25}$	single phase CC	32.4	32.5	9.3	25.8
N5	$(TiZr)_{50}Al_{10}Nb_{40}$	Overall	25.1	23.9	8.9	42.0
		BCC	25	24.4	9.2	41.4
		Al_3Zr_5	9.4	43.9	33.4	13.4
N6	$(TiZr)_{40}Al_{20}Nb_{40}$	overall	19.6	20.3	18.8	41.3
		BCC	24.1	17.6	12.2	46.1
		σ	13.9	22.4	27.0	36.7
		Al_3Zr_5	8.8	41.5	35.2	14.5

Table 4 Phase constituents and composition of phases in N alloys after 700°C annealing for 1500 h

Alloy	**Nominal Composition**	**Region/Phase**	**Overall/Phase Composition (at.%)**			
			Ti	**Zr**	**Al**	**Nb**
N0	$(Ti,Zr)_{50}Al_{25}Nb_{25}$	overall	25.4	24.9	23.8	26.0
		*BCC	35.3	13.9	15.9	34.8
		*Al_3Zr_5	21.5	29.8	27.3	21.4
N1	$(Ti,Zr)_{35}Al_{25}Nb_{40}$	overall	18.1	17.4	22.9	41.7
		σ	10.8	18.2	24.8	46.2
		BCC1	17.8	19.5	16.6	46.1
		Al_3Zr_5	8.3	45.0	29.0	17.6
		BCC2	19.6	4.8	5.9	69.7
N2	$(Ti,Zr)_{42.5}Al_{40}Nb_{17.5}$	overall	21.2	22.2	38.9	17.8
		*Al_3Zr_4	25.6	19.2	36.4	18.8
		σ	17.0	17.6	35.4	30.0
		Laves C14	9.9	32.9	55.6	1.6
		Al_3Zr_5	13.2	34.9	37.1	14.9
N3	$(Ti,Zr)_{65}Al_{25}Nb_{10}$	overall	32.5	33.1	24.0	10.4
		Al_3Zr_5	16.1	42.1	34.2	7.6
		BCC	32.1	29.4	21.7	16.9
		*$AlTi_3$	39.8	28.5	22.0	9.8
N4	$(Ti,Zr)_{65}Al_{10}Nb_{25}$	overall	32.1	32.4	9.4	26.0

DISTRIBUTION A: Distribution approved for public release.

		BCC	29.1	33.9	5.9	31.1
		ω	6.1	65.4	25.5	3.1
		Al_3Zr_5	11.3	45.0	35.1	8.6
N5	$(Ti,Zr)_{50}Al_{10}Nb_{40}$	overall	25.6	24.1	9.4	40.9
		BCC	27.8	19.4	5.1	47.8
		*ω	16.0	39.0	19.5	25.6
N6	$(Ti,Zr)_{40}Al_{20}Nb_{40}$	overall	19.6	20.7	18.1	41.6
		BCC1	21.2	20.3	14.4	44.1
		BCC2	18.7	5.5	4.0	71.8
		Al_3Zr_5	8.5	45.3	30.0	16.1

*The size of this phase is slightly smaller than the spacial resolution of EDS analysis, so the composition shown here could be affected by surrounding phases and is less accurate.

Table 5 Phase constituents and composition of phases in NT alloys after 1300°C annealing for 500 h

Alloy	**Nominal Composition**	**Phase**	**Overall/Phase Composition (at.%)**				
			Ti	**Zr**	**Al**	**Nb**	**Ta**
NT0	$(TiZr)_{50Al25}(NbTa)_{25}$	overall	25.7	26.5	23.1	12.3	12.4
		BCC	30.6	21.3	19.0	14.3	14.8
		Al_3Zr_5	12.0	41.5	34.5	6.7	5.3
NT1	$(TiZr)_{35Al25}(NbTa)_{40}$	overall	17.0	19.7	23.1	19.4	20.8
		BCC	21.9	9.6	17.3	24.2	27.0
		Al_3Zr_5	9.9	39.3	35.1	9.4	6.4
		σ	14.6	12.5	26.5	23.9	22.5
NT2	$(TiZr)_{35Al25}(NbTa)_{40}$	overall	21.3	22.6	39.4	8.5	8.3
		BCC	28.8	15.7	35.1	10.7	9.6
		Laves C14	11.7	31.9	49.4	3.7	3.3
		σ	19.3	9.9	32.3	17.9	20.6
		Al_3Zr_5	13.8	34.7	36.5	8.0	7.0
NT3	$(TiZr)_{65Al25}(NbTa)_{10}$	overall	33.0	32.2	24.2	5.4	5.1
		BCC	36.7	30.0	21.8	5.9	5.6
		Al_3Zr_5	15.3	42.7	35.2	3.8	3.0

DISTRIBUTION A: Distribution approved for public release.

NT4	$(TiZr)_{65Al10}(NbTa)_{25}$	single phase BCC	31.7	32.6	9.3	13.3	13.1
NT5	$(TiZr)_{50Al10}(NbTa)_{40}$	single phase BCC	25.3	24.8	9.3	20.4	20.2
NT6	$(TiZr)_{40Al20}(NbTa)_{40}$	overall	20.4	22.1	17.9	19.8	19.8
		BCC	23.3	17.2	13.8	22.8	22.9
		Al_3Zr_5	9.5	41.7	35.3	8.5	5.0

Table 6 Phase constituents and composition of phases in NT alloys after 1000°C annealing for 1000 h

Alloy	**Nominal Composition**	**Phase**	**Overall/Phase Composition (at.%)**				
			Ti	**Zr**	**Al**	**Nb**	**Ta**
NT0	$(TiZr)_{50Al25}(NbTa)_{25}$	overall	25.5	26.4	24	12	12.2
		BCC	28.7	22.7	21.2	13.7	13.7
		Al_3Zr_5	12.5	41.2	35.3	6.9	4.0
NT1	$(TiZr)_{35Al25}(NbTa)_{40}$	overall	16.8	19.9	24.1	19.9	19.3
		BCC	21.4	6.5	8.5	26.8	36.8
		σ	17.4	17.2	26.6	21.6	17.3
		Al_3Zr_5	11.8	40.1	35.4	8.1	4.6
NT2	$(TiZr)_{42.5Al40}(NbTa)_{17.5}$	overall	21.5	22.7	38.7	8.9	8.3
		BCC	25.3	13.8	34.6	12.5	13.7
		Al_3Zr_4	16.6	31.2	41.3	7.0	3.9
		Al_3Zr_5	19.1	33.1	36.7	5.3	5.9
		Laves C14	13.6	32.2	50.5	1.9	1.8
		σ	27.0	9.7	32.3	13.6	17.5
NT3	$(TiZr)_{65Al25}(NbTa)_{10}$	overall	33.4	32.3	23.6	5.6	5.1
		BCC	35.6	30.9	22.2	5.6	5.6
		Al_3Zr_5	15.4	43.2	35.3	3.6	2.5
NT4	$(TiZr)_{65Al10}(NbTa)_{25}$	single phase BCC	32.3	32.6	9.1	13.2	12.8
NT5	$(TiZr)_{50Al10}(NbTa)_{40}$	overall	24.6	25.6	9.5	20.3	19.9
		BCC1	25.8	28.7	10.1	19	16.4
		BCC2	24.5	16.5	6.2	25.1	27.8
		Al_3Zr_5	10.0	46.2	34.4	6.1	3.2

DISTRIBUTION A: Distribution approved for public release.

NT6	$(TiZr)_{40Al20}(NbTa)_{40}$	Overall	19.9	23.5	19.6	18.4	18.7
		BCC2	24.1	10.1	10.5	26.2	29.0
		BCC1	26.0	18.5	17.9	20.1	17.5
		Al_3Zr_5	11.3	41.3	35.1	8.2	4.1

Table 7 Phase constituents and composition of phases in NT alloys after 700°C annealing for 1500 h

Alloy	**Nominal Composition**	**Phase**	**Overall/Phase Composition (at.%)**				
			Ti	**Zr**	**Al**	**Nb**	**Ta**
NT0	$(TiZr)_{50Al25}(NbTa)_{25}$	overall	25.5	26.5	24.2	12.2	11.7
		AlTi3	46.2	14.2	21.0	10.6	8.1
		Al3Zr5	13.2	43.4	33.9	6.5	3.0
		BCC	22.1	9.3	8.0	26.0	34.7
NT1	$(TiZr)_{35Al25}(NbTa)_{40}$	overall	17.5	18.4	23.9	20.3	20.0
		σ	11.8	16.1	21.5	25.7	24.9
		BCC2	13.3	3.5	3.4	33.5	46.4
		BCC1	24.8	21.8	19.6	21.3	12.4
		Al3Zr5	12.1	43.1	27.0	11.0	6.7
NT2	$(TiZr)_{35Al25}(NbTa)_{40}$	overall	21.0	22.9	38.8	8.5	8.8
		BCC	27.6	16.9	34.9	10.5	10.1
		Laves C14	9.8	33.3	54.2	1.3	1.5
		σ	19.0	10.6	32.5	17.9	20.1
		Al3Zr4	15.2	31.9	41.3	6.4	5.2
		Al3Zr5	13.7	34.2	36.6	8.0	7.5
NT3	$(TiZr)_{65Al25}(NbTa)_{10}$	overall	33.6	32.6	23.4	5.4	4.9
		*BCC	32.4	25.2	18.0	10.9	13.5
		*Al3Zr5	20.1	39.6	32.3	4.7	3.3
		*AlTi3	39.9	30.0	23.4	3.7	3.1
		*ω	34.1	35.9	20.5	4.3	5.2
NT4	$(TiZr)_{65Al10}(NbTa)_{25}$	overall	32.8	33.2	9.1	12.4	12.5
		BCC1	31.6	42.4	6.3	12.1	7.6
		BCC2	24.7	7.9	1.2	27.9	38.3
		ω	6.6	67.6	23.5	1.2	0.9
		Al3Zr5	11.0	49.8	34.4	4.7	0.2
NT5	$(TiZr)_{50Al10}(NbTa)_{40}$	overall	26.0	24.7	8.9	19.1	21.3

DISTRIBUTION A: Distribution approved for public release.

		BCC2	21.6	7.0	0.9	33.2	37.4
		ω	6.4	66.0	25.3	1.9	0.4
		BCC1	30.0	45.0	6.4	12.3	6.2
		Al3Zr5	10.9	50.0	31.7	6.2	1.2
NT6	$(TiZr)_{40Al20}(NbTa)_{40}$	overall	20.7	21.0	18.5	19.5	20.4
		Al3Zr5	13.5	42.4	33.8	8.2	2.1
		BCC2	21.9	3.6	3.0	33.5	38.0
		(BCC1+ω)	16.2	30.5	25.0	17.7	10.6

*The size of this phase is slightly smaller than the spacial resolution of EDS analysis, so the composition shown here could be affected by surrounding phases and is less accurate.

- **What opportunities for training and professional development has the project provided?**

During the period of this project, we held weekly meetings to discuss the trend of data, solve the experiment problems and rearrange the schedule. Through this process, the participants can learn how to overcome the obstacles and cooperate in experiments.

By conducting the project, the participants can learn the fundamental knowledge of the HEA/RHEA and the advanced experimental process. From the knowledge side, they have learned the preliminary phase formation behavior and the basic concept of the phase diagram regarding HEA/RHEA. In addition, they can also understand the principle of alloying design, and the foundation of physical metallurgy. From the experimental side, the participants can become familiar with different instruments during the process. They learned to operate the vacuum arc melting (VAR) furnace to fabricate the alloys. In addition, they were also well-trained to conduct various analytical instruments (XRD, SEM, EDS, EBSD and TEM…, etc.) to extract the phase information in alloys.

- **How were the results disseminated to communities of interest?**

We plan to publish at least two papers in this regard.

- **What do you plan to do during the next reporting period to accomplish the goals and objectives?**

Nothing to Report

Products

The project produced key equilibrium phase data of two representative RHESA systems. Equilibrium phase types and phase compositions were determined, and the

location of the phase regions were reported and plotted on partial pseudo-ternary phase diagrams.

Participants & Other Collaborating Organizations

- **What individuals have worked on this project?**

  Name: Min-Hung Tsai
  Total Number of Months: 12
  Project Role: PI
  Contribution to Project: Administration and management, research conceptualization and experimental design, data analysis.

  Name: Yun-Syuan Chen
  Total Number of Months: 12
  Project Role: Grad Student
  Contribution to Project: Alloy fabrication, phase and microstructure identification (SEM/EDS, EBSD and XRD), data analysis.

  Name: An-Chen Fan
  Total Number of Months: 12
  Project Role: Grad Student
  Contribution to Project: Alloy fabrication, phase and microstructure identification (SEM/EDS, EBSD, XRD and TEM), data analysis.

  Name: Chih-Hao Hsu
  Total Number of Months: 12
  Project Role: Grad Student
  Contribution to Project: Alloy fabrication, phase and microstructure identification (SEM/EDS, EBSD and XRD), data analysis.

- **Has there been a change in the active other support of the PD/PI(s) or senior/key personnel since the last reporting period?**

  Nothing to Report.

- **What other organizations have been involved as partners?**

  Nothing to Report.

- **Have other collaborators or contacts been involved?**
  Nothing to Report.

Impact

- **What was the impact on the development of the principal discipline(s) of the project?**

Very recently, RHEAs with superalloy-like microstructure were invented and had drawn significant attention [17, 18]. They were named **refractory high-entropy superalloys** (RHESAs). RHESAs have a two-phases microstructure with discrete BCC nanoscale precipitates surrounded by thin channels of a B2 matrix, forming a basket-weave like structure with various morphologies [2, 3, 7, 14, 17-24]. This microstructure resembles the γ-γ' microstructure in the Ni-based superalloys. Indeed, RHESAs were reported to have higher high temperature strength than single-phased BCC RHEAs [19, 21]. Thus, RHESAs have the potential to operate at temperatures apparently higher than that of current Ni-based superalloys. However, the formation of this superalloy-like microstructure is quite unusual in RHEAs. This is because the vast majority of RHEAs were either single-phased BCC alloys or alloys containing BCC + other IMs [25]. Our own survey shows that up to now, less than thirty alloys simultaneously contain BCC and B2 phases.

Thus, a key issues in the development of RHESAs is the control of the ordered B2 phase. For example, the composition and temperature of B2 stability can have important effects. Moreover, the composition and temperature range of the B2+BCC two-phase field is also critical. Unfortunately, there is no existing phases diagrams for higher order systems. Thus, the lack of knowledge regarding the phase equilibria around B2 and the reaction pathways to form B2+BCC structure severely hinders the design of RHESAs. Since theoretical models and computational tools that can guide the design of RHESAs also rely on these information, the lack of such information also renders these tools useless.

In this work we obtained the key equilibrium phase information in the Ti-Zr-Al-Nb-Ta and the Ti-Zr-Al-Nb system. The Ti-Zr-Al-Nb-Ta system is of great importance because most reported RHESAs belong to this system or its derivative system. The most important finding in this work is surprising – no equilibrium B2 phase region was detected in both systems from 700-1300°C. This finding has important implications: the Ti-Zr-Al-Nb-Ta and the Ti-Zr-Al-Nb system are not good potential systems for high temperature applications since long term, high temperature (> 700°C) service will probably lead to melting of the B2 phase and thus disappearance of the superalloy-like microstructure. Since many other reported RHESAs were derivative systems of Ti-Zr-

Al-Nb-Ta (i.e., number of different principal element between the two systems is less than two), it is also possible that other reported RHESAs could also do not contain equilibrium B2 phase at temperatures above 700°C. Of course, this need future further investigation. Therefore, our work points to the urgent need of searching for systems with equilibrium B2 + BCC structure.

The discrepancy between our observation and the reported B2 phases in Ti-Zr-Al-Nb-Ta system is intriguing. One possibility is that the B2 phase previous authors observed is a metastable phase, since the annealing time is rather short (most < 100 h). Another important possibility is that the B2 phases observed was not examined by TEM, so the existence of interconnected structure was not reported. As mentioned previously, in many systems one of the phase in the interconnected structure went through ordering transition and transformed from BCC to B2 phase. Thus the reported B2 phase was actually formed during quenching.

- **What was the impact on teaching and educational experiences?**
  Nothing to Report.

- **What was the impact on physical, institutional, and information resources that form infrastructure?**
  Nothing to Report.

- **What was the impact on technology transfer?**
  Nothing to Report.

- **What was the impact on society beyond science and technology?**
  Nothing to Report.

- **What percentage of the award's budget was spent in foreign country(ies)?**
  The awards budget of this project was 100% spent in Taiwan.

Changes/Problems

The original end date was 09/29/2021. But due to the outbreak of COVID19 in Taiwan in 2021, user facilities of the analytical instruments (SEM/EDS/EBSD, TEM…etc.) in all universities/institutes were either closed or working only partially. Therefore, our access to the analytical instruments becomes severely limited. Consequently, we requested a no cost extension for six months (till Mar 29th, 2022).

DISTRIBUTION A: Distribution approved for public release.

Special Reporting Requirements

Nothing to report.

Budgetary Information

Nothing to report.

Project Outcomes

In this project, two series alloys (N and NT series) after 700, 1000 and 1300ºC prolong annealing were investigated. The equilibrium microstructure, phase constituents, and composition of phases in the six systems were probed. Based on the information, the partial ternary/pseudo-ternary phase diagrams around the B2 composition X_2AlY at different temperatures in the systems were discovered. Based on our investigation, no equilibrium B2 phase existed in the N and NT series alloys at 700-1300°C. The fact that the two series alloys did not contain equilibrium B2 phases suggests that the absence of B2 phase is probably true for all the whole Ti-Zr-Al-Nb-Ta and Ti-Zr-Al-Nb alloy systems, not just for the seven alloys. This finding has important implications: the Ti-Zr-Al-Nb-Ta and the Ti-Zr-Al-Nb system are not good potential systems for high temperature (> 700°C) applications since long term, since their lack of the B2 phase and the superalloy-like microstructure.

Our work has pointed to the urgent need of searching for systems with equilibrium B2 + BCC structure. Such information will further provide guidance for other RHESAs containing these subsystems, and lay the foundation for future development of theoretical models and computational tools.

Demographic Information for Significant Contributors

Name: Ming-Hung Tsai
Project Role: PI
Gender: Male
Race (select one or more): Asian
Disability Status: No

Name: Yun-Syuan Chen
Project Role: Graduate Student
Gender: Female
Race (select one or more): Asian
Disability Status: No

Name: An-Chen Fan

DISTRIBUTION A: Distribution approved for public release.

Project Role: Grad Student
Gender: Male
Race (select one or more): Asian
Disability Status: No

Name: Chih-Hao Hsu
Project Role: Grad Student
Gender: Male
Race (select one or more): Asian
Disability Status: No

References

[1] V. Soni, O. Senkov, J.-P. Couzinie, Y. Zheng, B. Gwalani, R. Banerjee, Materialia 9 (2020) 100569.
[2] V. Soni, B. Gwalani, T. Alam, S. Dasari, Y. Zheng, O.N. Senkov, D. Miracle, R. Banerjee, Acta Mater. 185 (2020) 89-97.
[3] V. Soni, O.N. Senkov, B. Gwalani, D.B. Miracle, R. Banerjee, Scientific reports 8 (2018) 1-10.
[4] Z. Wang, D. Jin, J. Han, Q. Wang, Z. Zhang, C. Dong, Crystals 11 (2021) 833.
[5] T.-Y. Liu, J.C. Huang, W.-S. Chuang, H.-S. Chou, J.-Y. Wei, C.-Y. Chao, Y.-C. Liao, J.S. Jang, Materials 12 (2019) 3508.
[6] S. Dasari, V. Soni, A. Sharma, O. Senkov, D. Miracle, H. Fraser, Y. Wang, R. Banerjee, Transactions of the Indian Institute of Metals 75 (2022) 907-916.
[7] T. Whitfield, E. Pickering, L. Owen, C. Jones, H. Stone, N. Jones, Materialia 13 (2020) 100858.
[8] T. Whitfield, E. Pickering, K. Christofidou, C. Jones, H. Stone, N. Jones, J. Alloys Compd. 818 (2020) 152935.
[9] T. Whitfield, G. Wise, H. Stone, N. Jones, Appl. Phys. Lett. 119 (2021) 211901.
[10] D.E. Laughlin, K. Hono, Physical metallurgy, Newnes, 2014.
[11] V. Soni, B. Gwalani, O.N. Senkov, B. Viswanathan, T. Alam, D.B. Miracle, R. Banerjee, J. Mater. Res. 33 (2018) 3235-3246.
[12] Y.-G. Dong, S. Chen, N.-N. Jia, Q.-H. Zhang, L. Wang, Y.-F. Xue, K. Jin, Tungsten 3 (2021) 406-414.
[13] Q. Wang, J. Han, Y. Liu, Z. Zhang, C. Dong, P.K. Liaw, Scr. Mater. 190 (2021) 40-45.
[14] T.E. Whitfield, E.J. Pickering, L.R. Owen, O.N. Senkov, D.B. Miracle, H.J. Stone, N.G. Jones, J. Alloys Compd. 857 (2021) 157583.

DISTRIBUTION A: Distribution approved for public release.

[15] T.E. Whitfield, H.J. Stone, C.N. Jones, N.G. Jones, Entropy 23 (2021) 80.
[16] H. Okamoto, T. Massalski, ASM International, Materials Park, OH, USA 1990) 12.
[17] O.N. Senkov, C. Woodward, D.B. Miracle, JOM 66 (2014) 2030-2042.
[18] J. Jensen, B. Welk, R. Williams, J. Sosa, D. Huber, O. Senkov, G. Viswanathan, H. Fraser, Scr. Mater. 121 (2016) 1-4.
[19] O.N. Senkov, D. Isheim, D.N. Seidman, A.L. Pilchak, Entropy 18 (2016) 102.
[20] N.Y. Yurchenko, N. Stepanov, S. Zherebtsov, M. Tikhonovsky, G. Salishchev, Mater. Sci. Eng. A 704 (2017) 82-90.
[21] O.N. Senkov, J.K. Jensen, A.L. Pilchak, D.B. Miracle, H.L. Fraser, Mater. Des. 139 (2018) 498-511.
[22]D.B. Miracle, M.H. Tsai, O.N. Senkov, V. Soni, R. Banerjee, Scr. Mater. 187 (2020) 445-452.
[23]D. Schliephake, A.E. Medvedev, M.K. Imran, S. Obert, D. Fabijanic, M. Heilmaier, A. Molotnikov, X. Wu, Scr. Mater. 173 (2019) 16-20.
[24] J. Wen, X. Chu, Y. Cao, N. Li, Metals 11 (2021) 514.
[25] O.N. Senkov, D.B. Miracle, K.J. Chaput, J.P. Couzinie, J. Mater. Res. 33 (2018) 3092-3128.

DISTRIBUTION A: Distribution approved for public release.